細胞移植1

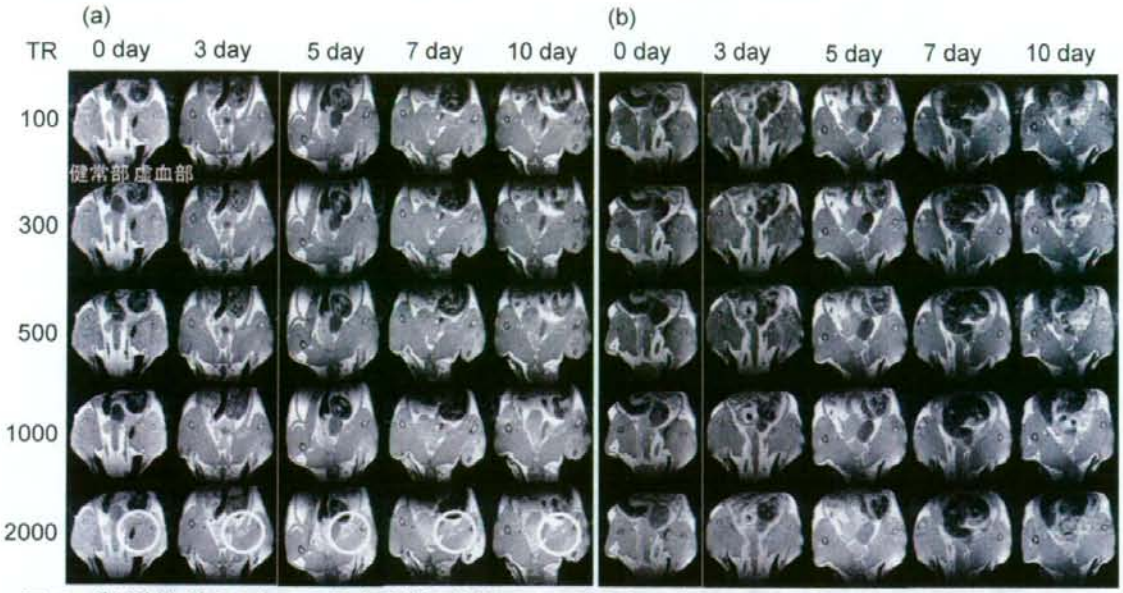


図 8. 造影剤を導入したラット間葉系幹細胞をラット下肢虚血モデルに細胞移植した後の MRI 撮像。ラット F344（14 weeks）下肢虚血モデルに対し、3X10$^7$ 個のラベル化細胞＋ボルヒール 100 μl を混合し、移植した。撮像は 2D-スピンエコー、スライス厚 1 mm で行った。(a) 細胞移植ラット (b) コントロール（ボルヒールのみ）

移植直後では、移植した細胞はコントラスト強く観察することができた。移植した細胞は 10 日目でほとんど見ることができなくなった。

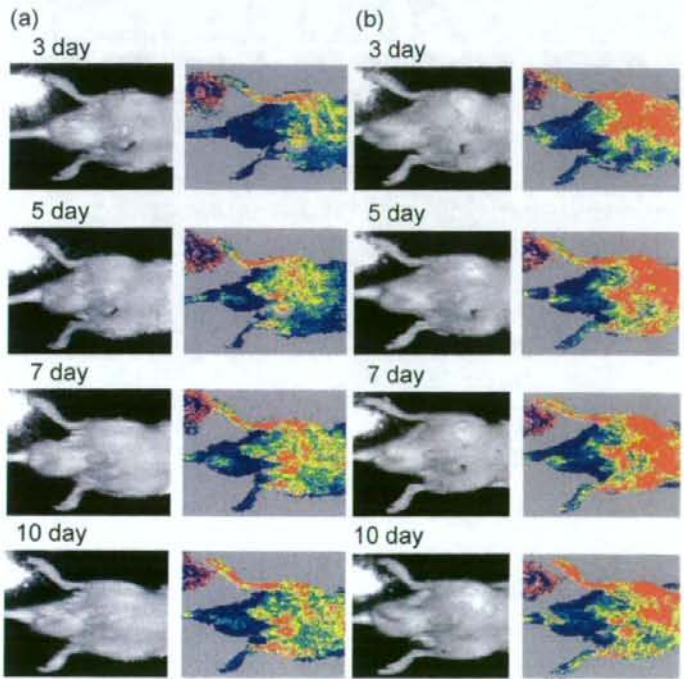


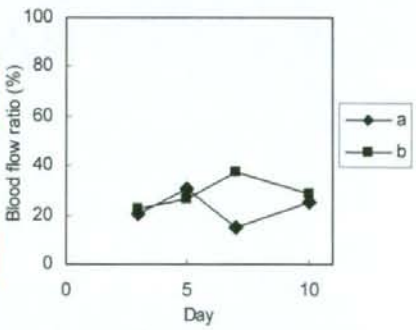


図 9. 細胞移植ラットの血流の変化。(a) 細胞移植ラット (b) コントロール

Blood flow ratio =

虚血部の血流 / 健常部の血流

細胞移植、コントロール共に血流の回復が見られた。血流の回復過程に差は見られなかった。

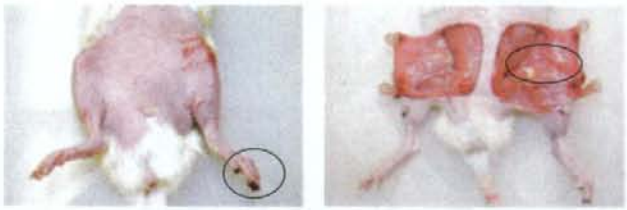

図 10. 細胞移植 20 日後のラットの様子
虚血部の足先は黒く変色し、虚血部の大腿筋肉は細くなっていた。

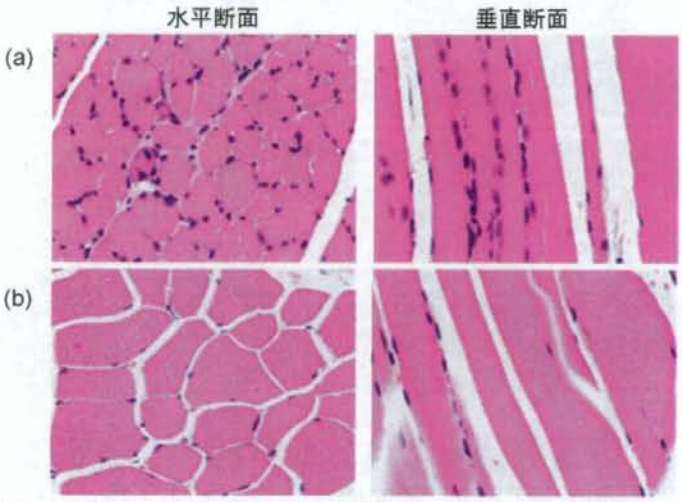


図 11. 細胞移植 20 日後のラットの大腿筋の HE 染色。(a) 虚血部 (b) 健常部
虚血部の筋線維の中央に核が見られ、筋線維周囲に核の増加が見られた。

---

**細胞移植2**

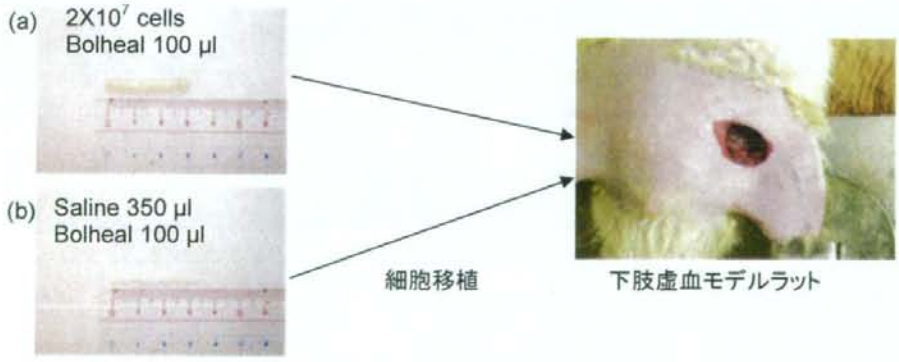


図 12. 細胞移植の流れ。2X10$^7$個のラット間葉系幹細胞を 100 µl のボルヒールに固めた。大腿動脈・静脈を切断し、下肢虚血モデルラットを作成した。切断した血管の痕に沿って、固めたゲルを置き、開口部を縫合した。(a) 細胞移植 (b) コントロール

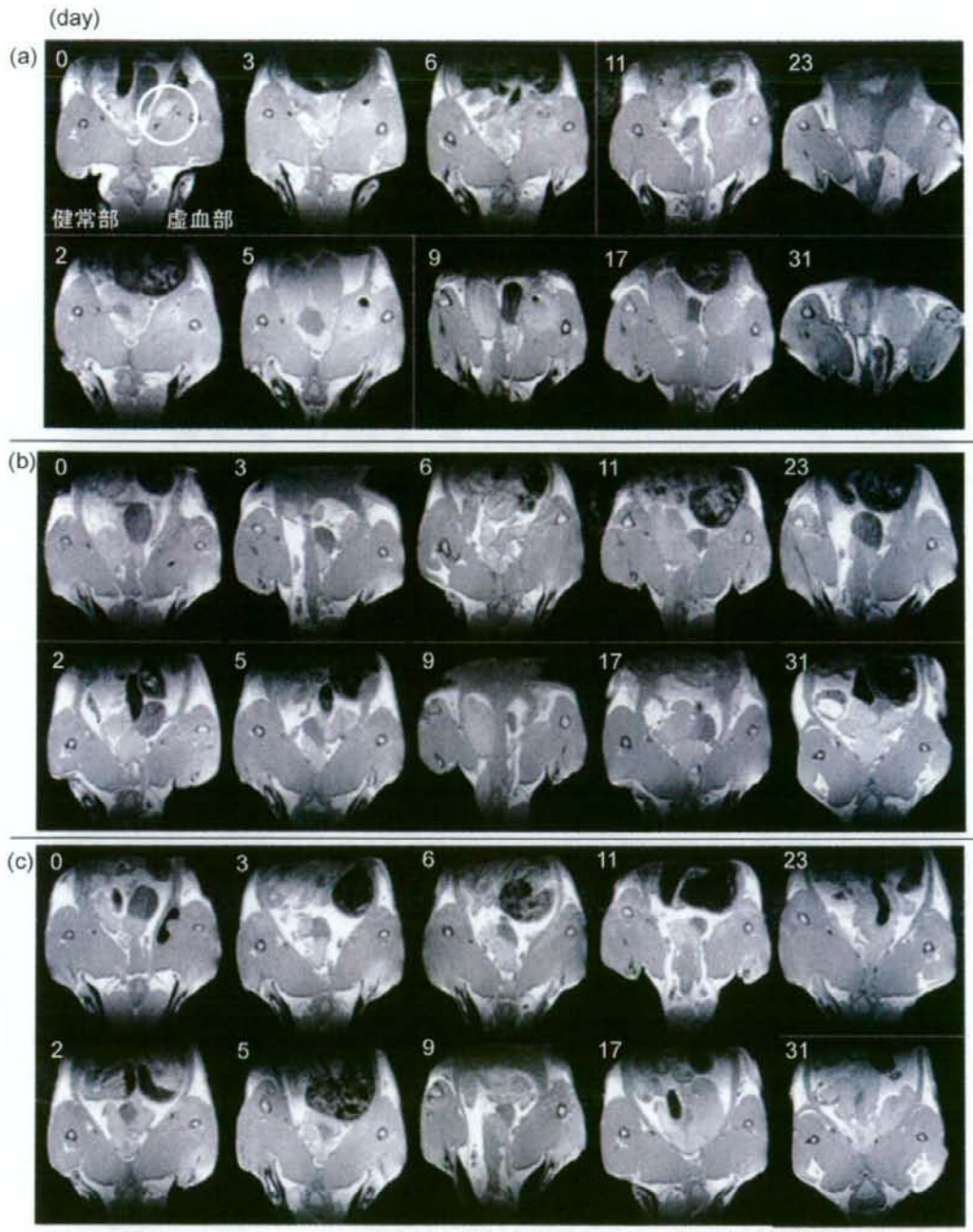


図 13. 造影剤を導入したラット間葉系幹細胞をラット下肢虚血モデルに細胞移植した後の MRI 撮像。撮像は 2D-スピンエコー、スライス厚 1 mm で行った。(a) 細胞移植ラット (b, c) コントロール(細胞なし)
細胞移植ラットでは移植細胞のコントラストの増強が見られた。一方、コントロールラットでは、コントラストに変化はなかった。

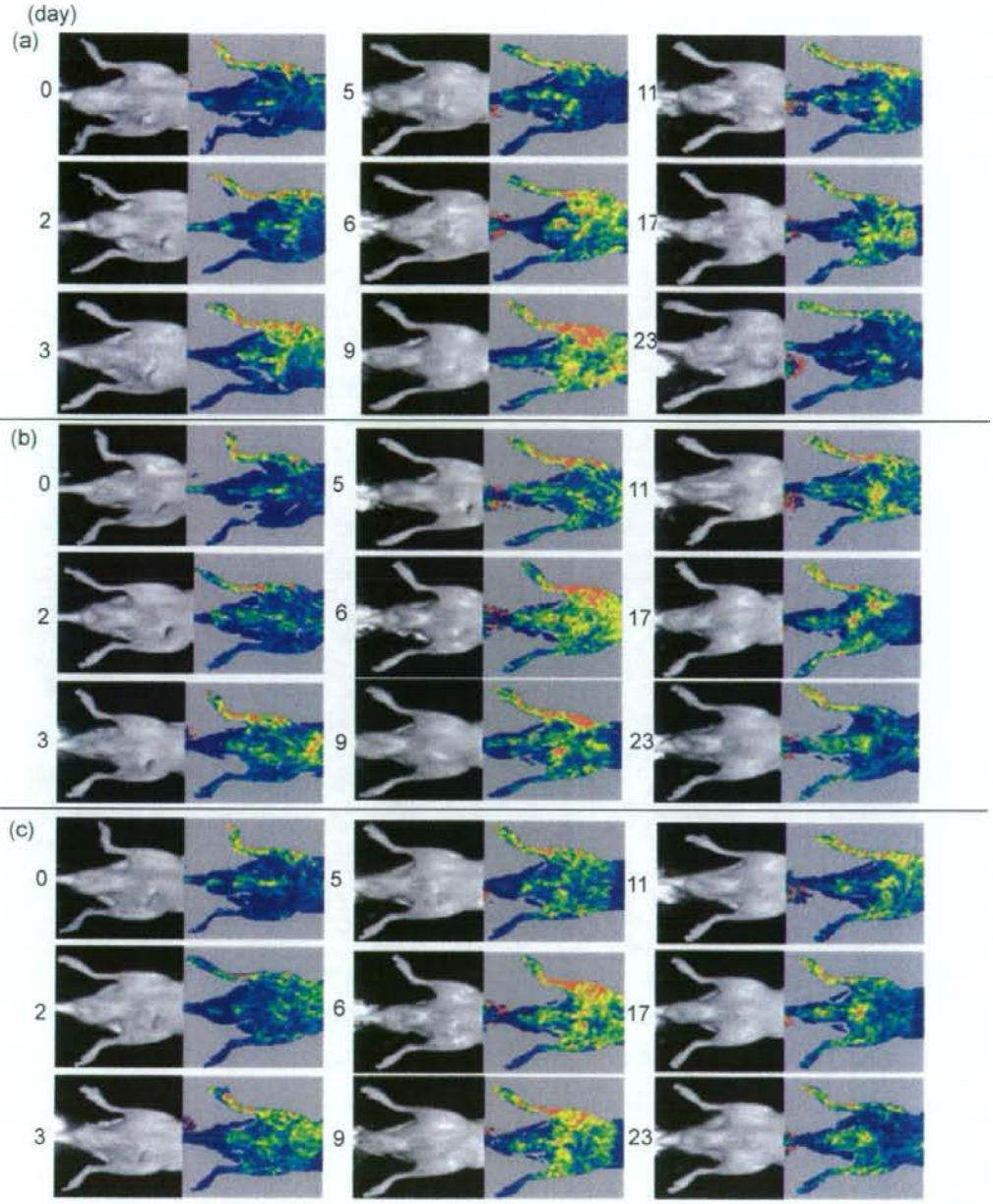
(day)
(a)
0
5
11
2
6
17
3
9
23
(b)
0
5
11
2
6
17
3
9
23
(c)
0
5
11
2
6
17
3
9
23

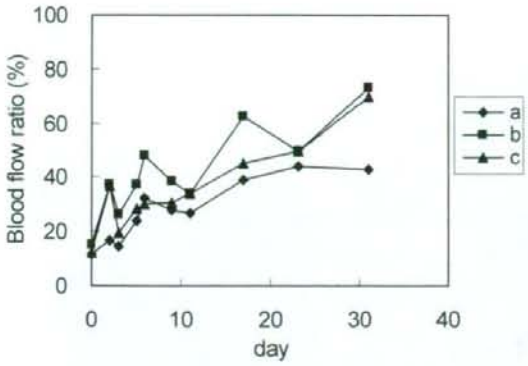


図 14. 血流の回復過程。(a) 細胞移植ラット (b, c) コントロール
Blood flow ratio = 虚血部の血流 / 健常部の血流

日数の経過に従って、虚血部の血流が回復していく様子が見られた。しかし、実験開始後 31 日後においても、虚血部は完全には回復していなかった。血流の回復過程はばらつきが大きい結果となった。

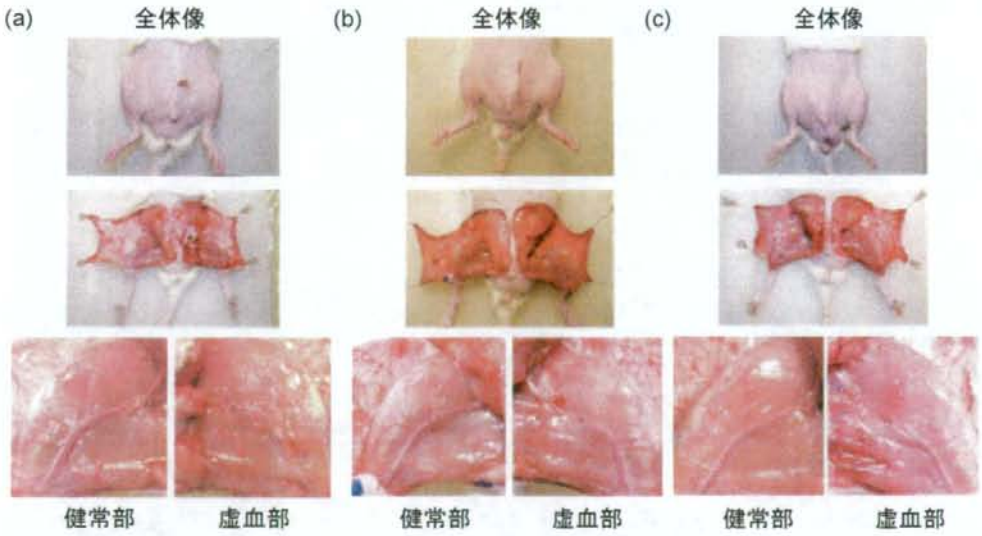


図 15. 細胞移植後 38 日後のラットの様子。(a) 細胞移植ラット (b, c) コントロール
虚血部は健常部に比べ、径の小さい血管が多く存在していた。細胞移植とコントロールラットでは、目視において差は見られなかった。

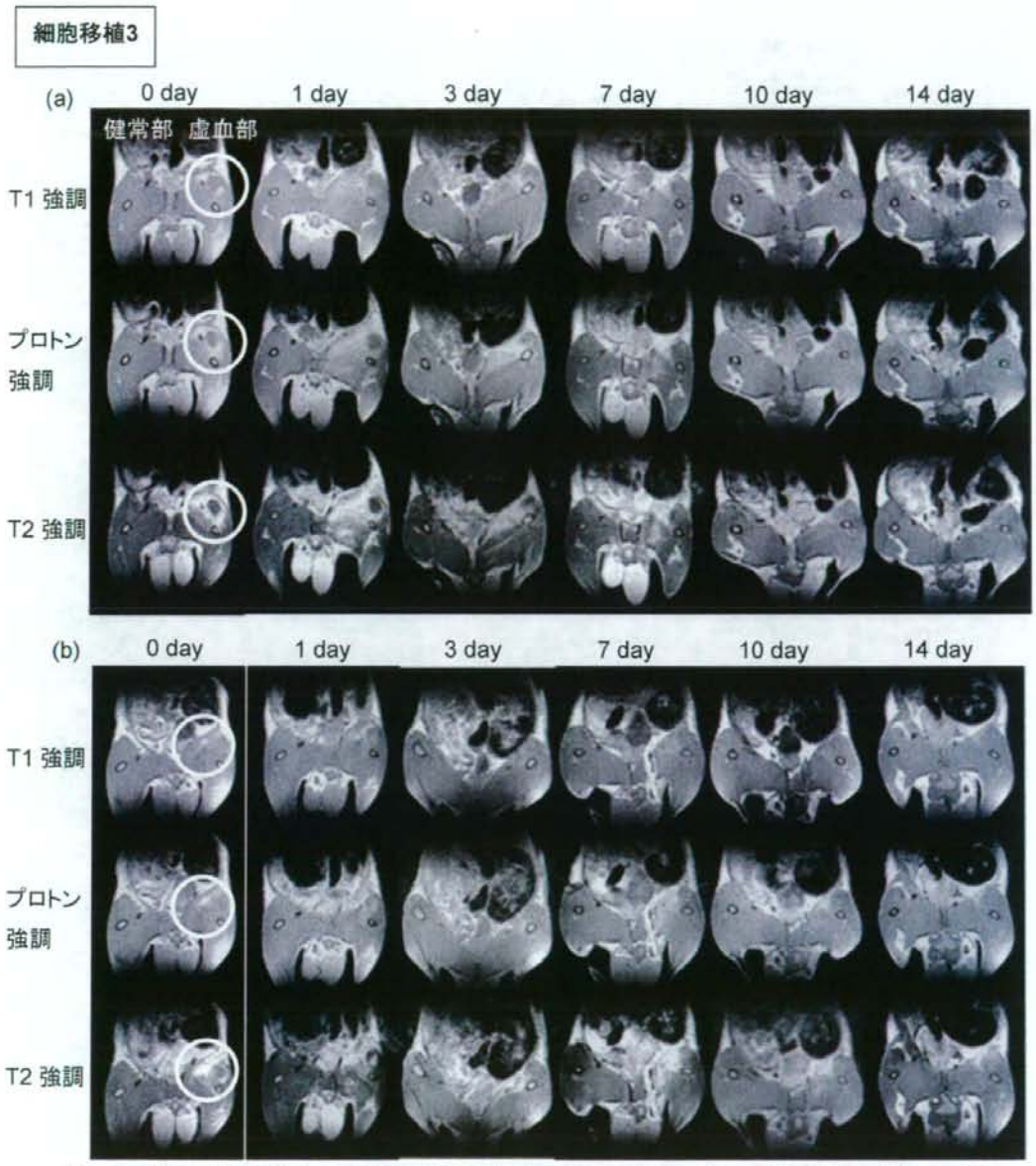


図 16. 造影剤を導入したラット間葉系幹細胞をラット下肢虚血モデルに細胞移植した後の MRI 撮像。撮像は 2D-スピンエコー、スライス厚 1 mm で行った。T1 強調:TE=9 ms、TR=1500 ms、プロトン強調: :TE=9 ms、TR=3000 ms、T2 強調:TE=30 ms、TR=3000 ms (a) 細胞移植ラット (b) コントロール(細胞なし)

移植した細胞は 7 日目まで確認することが可能であったが、10 日目では観察されなかった。

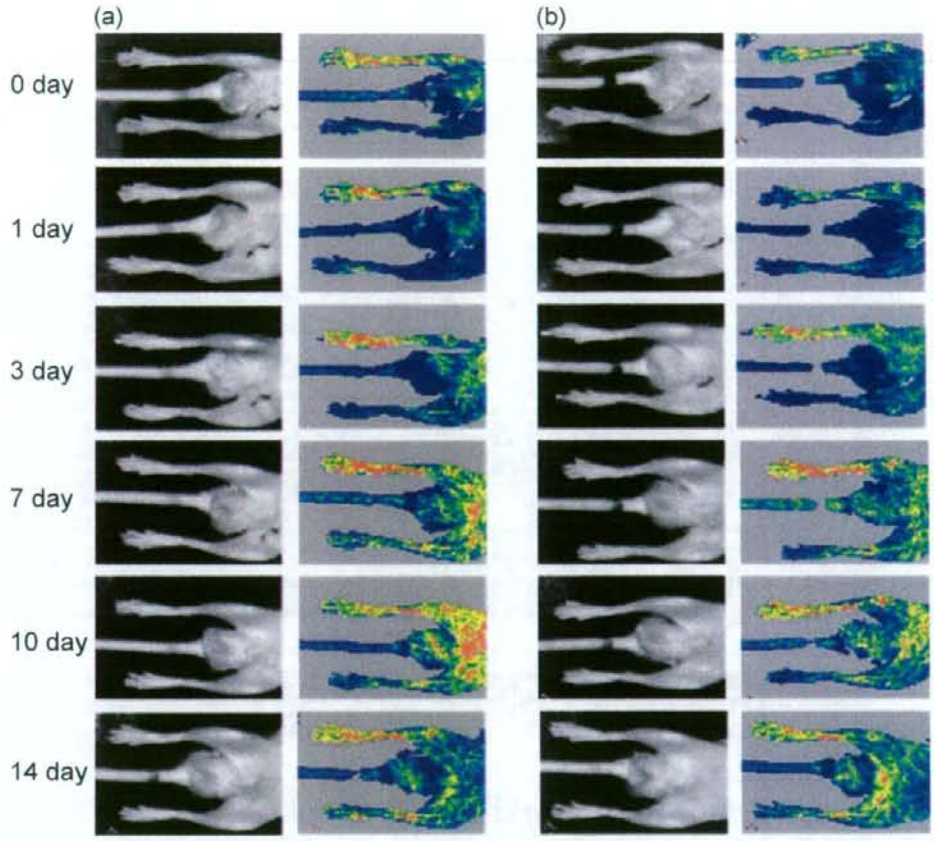


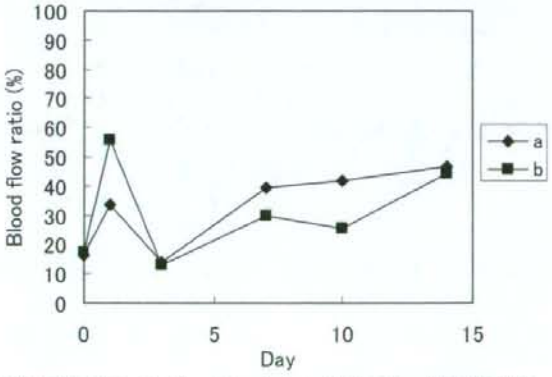


図 17. 血流の回復過程。(a) 細胞移植ラット (b) コントロール
Blood flow ratio = 虚血部の血流 / 健常部の血流

細胞を筋中にインジェクションした場合でも、細胞移植ラットとコントロールにほとんど差は見られなかった。

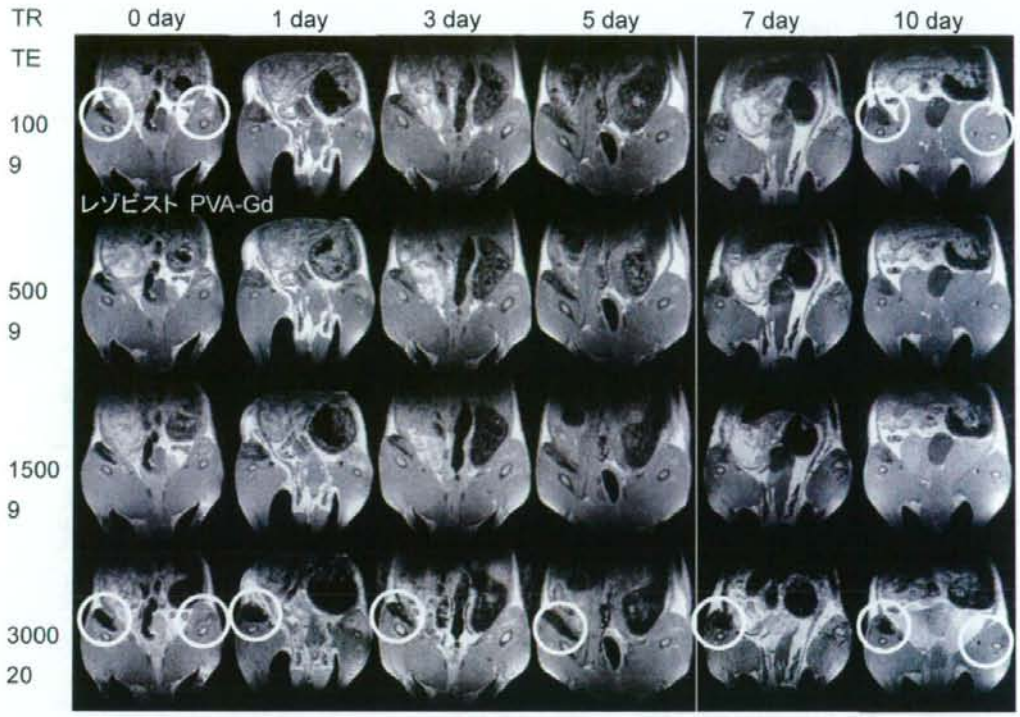


図 18. 造影剤水溶液を導入したラット大腿部筋中にインジェクションした後のMRI撮像。撮像は2D-スピンエコー、スライス厚 1 mm で行った。T1 強調:TE=9 ms、TR=100, 500, 1500 ms、T2 強調:TE=30 ms、TR=3000 ms

添5

研究成果の刊行に関する一覧表レイアウト（参考）

書籍

| 著者氏名 | 論文タイトル名 | 書籍全体の編集者名 | 書　籍　名 | 出版社名 | 出版地 | 出版年 | ページ |
|---|---|---|---|---|---|---|---|
| 馬原　淳<br>山岡哲二 | 幹細胞分離法とポピュレーション解析 | 秋吉一成<br>岸田晶夫 | 次世代医療のための高分子材料工学 | シーエムシー出版 | 東京 | 2008 | 168-177 |
| 中谷武嗣 | 心臓移植医療 | 国立がんセンター・国立循環器病センター | ビジュアル版「3大疾病の教科書がん・心臓病・脳卒中をストップ！」 | 三省堂 | 東京 | 2008 | 118-119 |
| 中谷武嗣 | 人工心臓 | 国立がんセンター・国立循環器病センター | ビジュアル版「3大疾病の教科書がん・心臓病・脳卒中をストップ！」 | 三省堂 | 東京 | 2008 | 120-121 |

雑誌

| 発表者氏名 | 論文タイトル名 | 発表誌名 | 巻号 | ページ | 出版年 |
|---|---|---|---|---|---|
| T. H. Ying | Scaffolds from electrospun polyhydroxyalkanoate copolymers: Fabrication, characterization, bioabsorption and tissue response | Biomaterials | 29 | 1307-1317 | 2008 |
| A. Miskon | Preservation of Porcine Hepatocytes in 3D Bioreactor at Room Temperature using Epigallocatechin-3-gallate | Tissue Engineering | E-pub, 2009 Jan 13 | — | 2009 |
| A. Miskon | Beating behavior of primary neonatal cardiomyocytes and cardiac-differentiated P19CL6 cells on different extramatrix components | Journal of Artificial Organs | In press | — | 2009 |
| D. Ishii | In Vivo Tissue Response and Degradation Behavior of PLLA and Stereocomplexed PLA Nanofibers | Biomacromolecules | 10(2) | 237-242 | 2009 |

| | | | | | |
|---|---|---|---|---|---|
| S. Kakinoki | Modification of PLA Scaffolds Using Bioactive Peptide-Oligo(Lactic Acid) Conjugates | The Japanese Peptide Society | — | 449-450 | 2009 |
| 山岡哲二 | 基礎医学「再生医療における工学技術」 | 教育セミナーテキスト | 第24号 | 5-12 | 2008 |
| Iida H | Absolute quantitation of myocardial blood flow with 201Tl and dynamic SPECT in canine: optimisation and validation of kinetic modelling. | Eur J Nucl Med Mol Imaging | 35 | 896-905 | 2008 |
| Kudomi N | Non-invasive estimation of hepatic blood perfusion from H215O PET images using tissue-derived arterial and portal input functions | Eur J Nucl Med Mol Imaging | 35 | 1899-911 | 2008 |
| Sato H | Comparison of Gd-DTPA-induced signal enhancements in rat brain C6 glioma among different pulse sequences in 3-Tesla magnetic resonance imaging | Acta Radiol | 49 | 172-9 | 2008 |
| Shidahara M | Optimal scan time of oxygen-15-labeled gas inhalation autoradiographic method for measurement of cerebral oxygen extraction fraction and cerebral oxygen metabolic rate | Ann Nucl Med | 22 | 667-75 | 2008 |
| Sohlberg A | Three-dimensional SPECT reconstruction with transmission-dependent scatter correction | Ann Nucl Med | 22 | 549-56 | 2008 |
| Sohlberg A | Acceleration of Monte Carlo-based scatter compensation for cardiac SPECT | Phys Med Biol | 53 | 277-85 | 2008 |
| Yamamoto A | Use of clinical MRI scanner for pre-clinical research on rats | Radiological Physics and Technology | — | — | 2008 |

| | | | | | |
|---|---|---|---|---|---|
| Yokoyama I | Heart and Brain Circulation and CO2 in Healthy Men | Acta Physiol (Oxf) | 193 | 303-8 | 2008 |
| Zeniya T | Clinical usability of a compact high resolution detector for high resolution and quantitative SPECT imaging in a selected small ROI | EEE 2008 Nuclear Science Symposium Conference Record | – | 4257-59 | 2008 |
| 越野 一博 | 心筋PET検査の有用性 | 臨床画像 | 24 | 157-64 | 2008 |
| 銭谷 勉 | 高解像度定量ピンホールSPECTイメージング—小動物から臨床へ— | 映像情報Medical | 40 | 1210-15 | 2008 |
| 銭谷 勉 | SPECTイメージング | 遺伝子医学MOOK9号「分子イメージング技術」 | – | 75-81 | 2008 |
| 飯田 秀博 | 特集/分子イメージング時代の画像解析・データ解析の新しい視点-特集のねらい-New Image Processing Technologies for Clinical and Pre-clinical Molecurlar Imaging | Med Imag Tech | 26 | 1-2 | 2008 |
| 林 拓也 | 神経画像法を用いた虚血性脳疾患の前臨床・臨床試験と病態把握 | 循環器病研究の進歩 | 48 | 79-86 | 2008 |
| Mano A | Which factors predict the recovery of natural heart function after insertion of a left ventricular assist system? | Journal of Heart and Lung Ttansplantation | 27 | 869-874 | 2008 |
| Miyata S | Heparin-induced thrombocytopenia clinical studies and the efficacy of argatroban in Japan | Semin Thromb Hemost | 34 | 37-47 | 2008 |

| | | | | | |
|---|---|---|---|---|---|
| Morimoto Y | Hemostatic management during oral surgery in patients with a left-ventricular assist system undergoing high-level anticoagulant therapy: efficacy of low molecular weight heparin | Surg J Oral Maxillofac | 66 | 568-571 | 2008 |
| 小林奈歩 | 心臓移植適応について検討した患者の予後 −院内臓器移植医学的適応症例検討会に小児科から提示した症例− | 日本小児循環器学会雑誌 | 24 | 628-635 | 2008 |
| 中谷武嗣 | 補助人工心臓の現状と今後の展望 | 呼吸と循環 | 56 | 377-382 | 2008 |
| 中谷武嗣 | 循環動態維持を目的とした薬物療法と補助循環法 | ICUとCCU | 31 | 1061-1067 | 2008 |
| 中谷武嗣 | 対外設置型補助人工心臓 −東洋紡補助人工心臓− | Clinical Engineering | 19 | 618-622 | 2008 |
| 中谷武嗣 | 心不全の機械的補助最前線 | Current Therapy | 26 | 955-958 | 2008 |
| 中谷武嗣 | 心臓移植における保存法 | 移植 | 43 | 336-341 | 2008 |
| 橘　洋一 | 展望　心臓疾患における幹細胞移植治療の現状とその追跡法 | ISOTPOE NEWS | 649 | 2-7 | 2008 |
| 山岡哲二 | 最近の進歩　「細胞移植と分子イメージング」 | 人工臓器 | 37(3) | 179-181 | 2008 |

学会発表

| 演者 | 演題名 | 学会名 | 場所 | 開催年月日 |
|---|---|---|---|---|
| 藤里俊哉 | 生体由来素材スキャフォールドを用いた臓組織再生 | 第36回人工心臓と補助循環懇話会 | 越後湯沢 | 2008.3.7-8 |
| 橘　洋一 | 感温性ポリエチレンイミン誘導体を用いた遺伝子導入 | 第8回 遺伝子・デリバリー研究会シンポジウム | 大阪 | 2008.5.9 |
| 橘　洋一 | MRI細胞トラッキング技術を用いた下肢虚血細胞移植におけるEBMの確立 | 第３回日本分子イメージング学会 | 埼玉 | 2008.5.22-23 |

| | | | | |
|---|---|---|---|---|
| 東　晃至 | ソノポレーション法を用いた高分子造影剤の細胞内導入 | 第57回高分子学会年次大会 | 横浜 | 2008.5.28-30 |
| Tetsuji Yamaoka | In Vivo Tracking of the Transplanted Cells Using a Novel Polyric Contrast Agent, | 8th World Biomaterials Congress | Amsterdam | 2008.5.28-6.1 |
| 山岡哲二 | 新規な生細胞追跡MRIプローブによる移植幹細胞のin vivo イメージング | 第24回日本DDS学会 | 東京 | 2008.6.29-30 |
| 橘　洋一 | 移植細胞の長期追跡を目的とした高分子MR用造影剤の開発 | 第24回日本DDS学会 | 東京 | 2008.6.29-30 |
| 橘　洋一 | ポリエチレングリコールを担体とした細胞追跡用MRI造影剤の開発 | 第36回日本磁気共鳴医学会大会 | 旭川4 | 2008.9.11-13 |
| 中谷武嗣 | 心移植：既存抗体、産生抗体のモニタリングと移植後の管理 | 第44回日本移植学会総会 | 大阪 | 2008.9.19-21 |
| 橘　洋一 | 下肢虚血ラットへのMSC移植におけるMRI細胞トラッキング | 第57回高分子討論会 | 大阪 | 2008.9.24-26 |
| 東　晃至 | 分子量の異なる高分子化MRI造影剤を用いた細胞標識とin vivoイメージング | 第57回高分子討論会 | 大阪 | 2008.9.24-26 |
| T. Yamaoka | Novel biomaterirals for cell transplantation | TERMIS-AP 2008 | Taipei | 2008.11.6-8 |
| 中谷武嗣 | 再生医学・生体組織工学1 | 第46回日本人工臓器学会大会 | 東京 | 2008.11.27-29 |
| 中谷武嗣 | わが国における補助人工心臓の将来 | 第46回日本人工臓器学会大会 | 東京 | 2008.11.27-29 |
| 山岡哲二 | 細胞移植医療における細胞のin vivoイメージングへ向けた新規細胞ラベル化用MRI造影剤の開発 | 第三回　ナノバイオテクノロジー連携群　成果報告会 | 東京 | 2009.1.28 |

The propagation of an error in $k_g$ and delay time to blood flow estimation was simulated. The sequence of steps in this procedure is simplified in Fig. 2a and b. For $k_g$, simulated portal input curves were created from the selected arterial curve by changing $k_g$ from 0.35 to 0.65/min for error simulation in $k_g$, and combinations of the arterial and simulated portal vein curves were used as the simulated DIF. Sets of tissue TACs were generated from these simulated DIFs, with the same assumptions of $f_a$ and $r$ as given above. In turn, each set for each $k_g$ was used to back-estimate DIF (arterial and portal components), fixing $k_g$ as 0.5/min in this process as presented above. Finally, $f_a$ and $f_p$ were calculated from estimated DIFs for each $k_g$ by the Gauss–Newton non-linear fitting method in the interactive modeling and data analysis system called PyBLD (http://homepage2.nifty.com/peco/pybld/pybld.html) [5] using Eq. 4. For delay time, simulated portal input curves were created from the selected arterial curve by shifting the time from 0 to 10 s, and combinations of the arterial and simulated portal vein curves were used as the simulated DIF. Sets of tissue TACs were generated as above. In turn, each set for each delay time was used to back-estimate DIF fixing time delay as 0.0 s. Finally, $f_a$ and $f_p$ were calculated from estimated DIFs for each delay time. Mean of percent difference between computed and assumed ('true') flow values are presented as a function of $k_g$ and delay time.

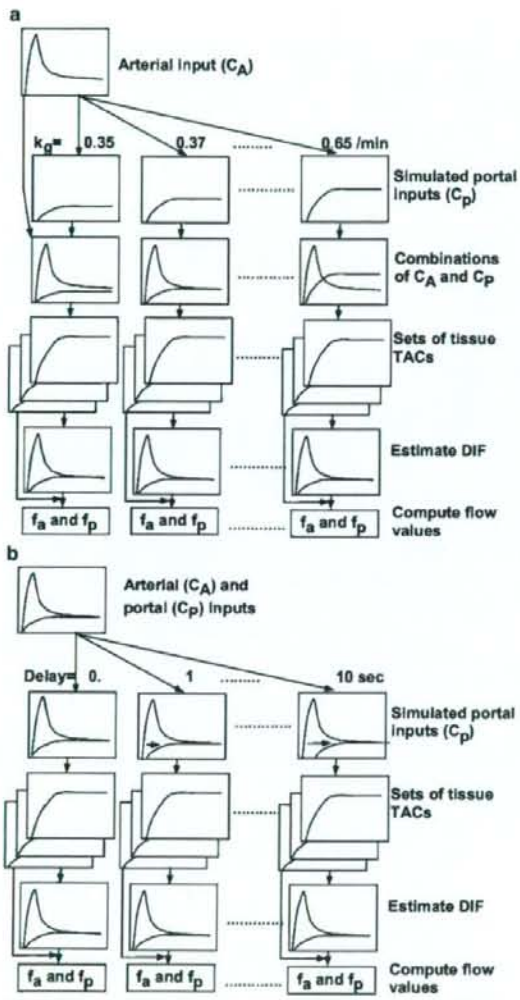


**Fig. 2** Schematic diagram of the procedure to analyze error sensitivity in hepatic arterial ($f_a$) and portal flow ($f_p$) values against assumed $k_g$ (**a**) and time delay (**b**). Portal input curves were created by changing the value of $k_g$ from 0.35 to 0.65/min in (**a**) and by shifting the time from 0 to 10 s in (**b**), respectively, and combinations of the arterial ($C_A$) and simulated portal ($C_P$) curves were used as the simulated dual input functions (*DIF*). Sets of tissue time–activity curves (*TAC*) were generated from these simulated DIFs by assuming ten values of $f_a$ from 13 to 17 ml/min/100 g. In turn, each set of tissue TACs was used to back-estimate DIF fixing $k_g$ as 0.5/min and time delay as 0.0 s. Finally, $f_a$ and $f_p$ were calculated from estimated DIFs for each $k_g$ and delay time

To analyze the influence of noise versus number of TACs on the accuracy of the method was explored. As shown by Edward et al. [7], as the noise on tissue TACs increased, the standard deviation of uptake ratio of tracer increased; as more regions were used, the standard deviation tended to decrease. However, if the number of TACs is larger, the noise on tissue is also large and vice versa. Our simulation was intended to reveal an optimal number of tissue TACs to be extracted from the whole region of the liver. The procedure is summarized in Fig. 3. First, tissue TACs with noise were generated as follows: Gaussian noise at peak was imposed on the set of ten hepatic tissue TACs generated above. Two levels of noise were introduced, corresponding to 10% and 20% of counts at the level of the peak and 10% and 20% each of the square root of counts at the other points. This procedure was repeated 100 times and 100 sets of noisy tissue TACs, embracing a total of 1,000 pixels obtained. Next, the $i$th set of tissue TACs in $k$th frame with $f_a$ defined as $C_{fa}^{i,k}$ were summed for same $f_a$ as

$$\overline{C}_{fa}^{k} = \frac{1}{N_T}\sum_{i}^{N_T} C_{fa}^{i,k} \qquad (7)$$

where $N_T$ indicates the summed number of tissue TACs and corresponds to the summed number of pixels. $N_T$ were set to 5, 10, 20, 50, 100, and 200, corresponding to a number of tissue TACs ($N_{tis}$) of 200, 100, 50, 20, 10, and 5, respectively. Here, when $N_T$ was 200, the 100 tissue TACs were summed as $N_T$=100 and additionally combinations of $f_a$=13 and 13.5, 14 and 14.5, 15 and 15, 15.5 and 16, and 16.5 and 17 ml/min/100 g were summed. For each $N_{tis}$ and

Fig. 1. Multiple tissue time–activity curves (TAC) from liver image were used to estimate the input functions. First, the model function in Eq. 4 was individually fitted to tissue TACs, assuming that $k_g$ in Eq. 2 is constant by a non-linear fitting method (variable-metric method in the PAW environment: version 2.13/08 [http://wwwasd.web.cern.ch/wwwasd/paw/]), and the set of seven parameters of $A$, $t_1$, $t_2$, $K_e(1+\alpha)$, $f_a$, $f_p$, and $V_0$ in Eqs. 1 and 4 was obtained for each tissue TAC. Then, means and standard deviations of $t_1$, $t_2$, and $r_a(=f_a/(f_a+f_p))$ were calculated, and the tissue TACs with values of $t_1$ or $t_2>1$ standard deviation of respective means were excluded to avoid the potential influence of TACs outside the liver. In the second step, assuming that all parts of the liver share the same input functions, values of $t_1$, $t_2$, and $r_a$ were fixed to their means, and the other two parameters ($A$ and $K_e(1+\alpha)$) were estimated by minimizing the following equation:

$$S^2 = \sum_{i\in Tis}\sum_{k}\left(C_{PET}^{i,k} - \left((1-V_0^i)\left(f_a^i C_A(t) + f_p^i C_P(t)\right) \otimes e^{-k_2^i t} + V_0^i C_{input}(t)\right)\right)^2 \quad (6)$$

where $C_{PET}^{i,k}$ is the tissue TAC for $k$th frame in $i$th tissue region of interest, $t$ is the corresponding time of $k$th frame, and $f_a^i$, $f_p^i(=f_a^i(1-r_a)/r_a)$ and $V_0^i$ are values of arterial and portal vein blood flows and of blood volume for $i$th tissue, respectively. In this procedure, $S^2$ was minimized by the grid search method *to* avoid dependency of initial guess, where $S^2$ was calculated for 1,000 discrete values of both $A$ and $K_e(1+\alpha)$ between ranges of three standard deviations from respective mean values, omitting the negative value. In this procedure, for a given input function, i.e., given $A$ and $K_e(1+\alpha)$, $f_a$ and $V_0$ for each TAC were computed by the grid search method, with acceptable ranges of 0–100 ml/min/g and 0–1 ml/ml, and steps of 1 ml/min/g and 0.01 ml/ml, respectively, and then substituted in Eq. 6. Finally, the image-based input function was obtained by substituting the estimated parameters into Eq. 1.

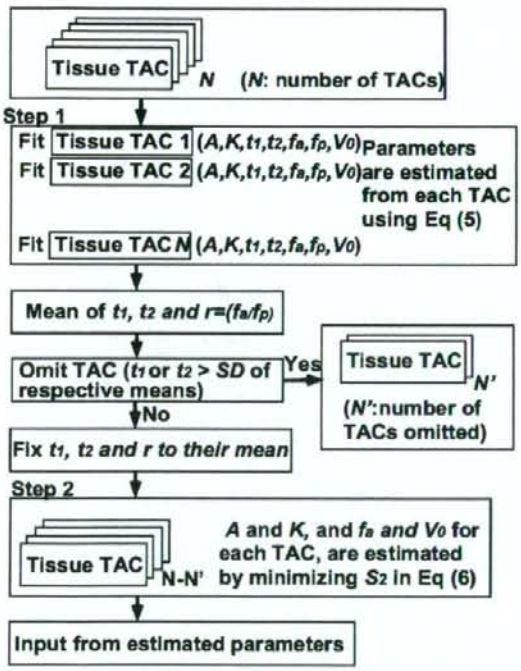


**Fig. 1** A schematic diagram of the procedure to estimate the input functions using multiple tissue TACs. *Step 1* The model function (Eq. 4) was individually fitted to $N$ tissue time–activity curves (*TAC*). Then, means and standard deviations of $t_1$, $t_2$, and $r_a$ were calculated, and the tissue TACs with values of $t_1$ or $t_2>1$ standard deviation of respective means were excluded (indicated as $N'$ TACs) to avoid the potential influence of TACs outside the liver. In the second step, assuming that all parts of the liver share the same input functions, values of $t_1$, $t_2$, and $r_a$ were fixed to their means, and the other two parameters ($A$ and $K_e(1+\alpha)$) were estimated by minimizing Eq. 6 by the grid search method. Finally, the image-based input function was obtained by substituting the estimated parameters into Eq. 1

## Simulation study

The present method for generating portal vein input assumes that the diffusion rate in the gut system, $k_g$, is a fix constant, and there is no time delay between portal and arterial blood. It is not a priori known how these assumed factors degrade the accuracy of estimated DIF and flow. Moreover, tissue TACs from PET images convey some degree of noise, and the accuracy of the estimated input function might depend on either the degree of noise, or the applied number of tissue TACs, or both. A simulation study was designed to reveal the influence of the above elements on the accuracy of the current method.

To this purpose, we selected one arterial curve from one of the present experiments. First, a portal input curve was created by assuming $k_g=0.5$/min, corresponding to the estimated mean in all animals. The combination of these arterial and portal vein curves was treated as the 'true DIF'. In the present experimental study, the average of activity concentrations in an area of the summed image was distributed with a 20% range around the mean for the whole liver, and this percentage was independent of the size of the selected areas in regions >50 pixels. This supports the assumption that flow values in the liver distribute around a 20% range around a mean of arterial flow of 15 ml/min/100 g [22]. Thus, by assuming ten values of $f_a$ as 13, 13.5, 14, 14.5, 15, 15, 15.5, 16, 16.5, and 17 ml/min/100 g, and ratio $r(=f_p/f_a)=6$ [22], one set of ten hepatic tissue TACs was generated from the true DIF using Eq. 6.

perfusion, representing a prognostic indicator and responding to disease amelioration [4, 10, 19, 21, 28–31, 35]. Positron emission tomography (PET) and $^{15}O$-labeled water ($H_2{}^{15}O$) enable to assess hepatic perfusion quantitatively [29, 30, 35], as based on tracer kinetic modeling, requiring the notion of the time variation of radiotracer concentrations in the liver tissue and in the blood entering the organ (input function).

The liver is characterized by a dual blood supply, comprising the hepatic artery and the portal vein, draining venous blood from the gastrointestinal tract. Thus, in the modeling of PET data from liver, two blood time–activity curves are required to represent the input function (dual input function [DIF]). However, blood withdrawal from a peripheral artery [8, 9, 16, 17, 26, 33] is not always successful and risk-free, and it requires careful correction in time delay between the sampling site and the tissue. More importantly, the portal vein cannot be accessed from any peripheral site, making its blood collection impractical in humans.

The aim of the present study was to develop a new technique to estimate the two components of the DIF non-invasively from dynamic $H_2{}^{15}O$ PET images. The present method was characterized by use of a model input function to create a tissue model function, which was used to simultaneously fit multiple tissue curves from PET image. The parameter obtained in the input function model reproduced the input function. Computer simulation studies were performed to examine the magnitude of potential biases in the parameter estimates caused by the inherent assumptions and to optimize the extraction of multiple tissue curves from the image. The present investigation was conducted in pigs because the comparison between measured and estimated values necessitated deep catheterization and invasive Doppler flow measurements.

## Materials and methods

### Theory and computation of non-invasive DIF

A model function was created to shape the input function according to the dose of tracer, administration process, body weight, and physiological state in each subject [18]. The model function introduced is

$$\begin{aligned} C_A(t) &= 0. && (t < t_1) \\ &= \frac{A}{K_e^2(1+\alpha)^2}\left(1 - \exp\left(K_e(1+\alpha)(t_1 - t)\right)\right) && (t_1 \le t \le t_2) \\ &= \frac{A}{K_e^2(1+\alpha)^2}\left(\exp\left(K_e(1+\alpha)(t_1 - t_2)\right) + \exp\left(K_e(1+\alpha)(t_2 - t)\right) - 2\cdot\exp\left(K_e(1+\alpha)(t_1 - t)\right)\right) && (t > t_2) \end{aligned} \quad (1)$$

Details of the model function are given in the Appendix. Briefly, $A$ indicates the height, and $t_1$ and $t_2-t_1$ indicate the appearance time of tracer and administration duration, respectively. $K_e$ (ml/min) and $K_1(=\alpha K_e)$ (ml/min) represent the tracer bidirectional diffusion rates between arterial blood and whole body interstitial spaces, respectively.

The portal vein blood model function was generated by introducing the gut compartment model [29–31, 35], that is, a single compartment model between arterial blood and gut compartment, assuming no difference in appearance time between arterial and portal blood (or delay time of portal input), with diffusion rate $k_g$ in the gut system as

$$C_P(t) = k_g C_A(t) \otimes e^{-k_g t} \quad (2)$$

Using these arterial and portal input model functions, the tissue response function can be expressed by assuming a single tissue compartment model [29–30, 35] and that tracers in arterial and portal blood were well mixed before exchange with liver tissue as

$$C_{TIS}(t) = \left(f_a C_A(t) + f_p C_P(t)\right) \otimes e^{-k_2 t} \quad (3)$$

where $k_2$ is defined as $(f_a+f_p)/V_L$, and $V_L$ (ml/g) is the distribution volume of water between blood and tissue. In the present study, $V_L$ was fixed to 0.7 ml/g, which was suggested to fix in a sensitivity analysis by Ziegler et al. [35] and was obtained as 0.71±0.03 ml/g for same subjects in our preliminary evaluation using measured blood input functions. Including a blood volume term into this equation, the model function for liver tracer concentrations, as measured by PET ($C_{PET}$), can be expressed as

$$C_{PET}(t) = (1 - V_0)\left(f_a C_A(t) + f_p C_P(t)\right) \otimes e^{-k_2 t} + V_0 C_{input}(t) \quad (4)$$

where $C_{input}(t)$ is defined as

$$C_{input}(t) = r_a C_A(t) + r_p C_P(t) \quad (5)$$

where $r_a$ and $r_p$ are arterial ($f_a$ ml/min/g) and portal vein blood flow ($f_p$ ml/min/g) ratios to total hepatic flow, i.e., $r_a=f_a/(f_a+f_p)$ and $r_p=f_p/(f_a+f_p)$ [35]. The flow chart to estimate input functions in this procedure is simplified in

Eur J Nucl Med Mol Imaging (2008) 35:1899–1911
DOI 10.1007/s00259-008-0796-z

ORIGINAL ARTICLE

# Non-invasive estimation of hepatic blood perfusion from $H_2{}^{15}O$ PET images using tissue-derived arterial and portal input functions

**N. Kudomi · L. Slimani · M. J. Järvisalo · J. Kiss · R. Lautamäki · G. A. Naum · T. Savunen · J. Knuuti · H. Iida · P. Nuutila · P. Iozzo**

Received: 30 August 2007 / Accepted: 25 March 2008 / Published online: 6 May 2008


**Abstract**
*Purpose* The liver is perfused through the portal vein and the hepatic artery. When its perfusion is assessed using positron emission tomography (PET) and $^{15}O$-labeled water ($H_2{}^{15}O$), calculations require a dual blood input function (DIF), i.e., arterial and portal blood activity curves. The former can be generally obtained invasively, but blood withdrawal from the portal vein is not feasible in humans. The aim of the present study was to develop a new technique to estimate quantitative liver perfusion from $H_2{}^{15}O$ PET images with a completely non-invasive approach.

*Methods* We studied normal pigs ($n$=14) in which arterial and portal blood tracer concentrations and Doppler ultrasonography flow rates were determined invasively to serve as reference measurements. Our technique consisted of using model DIF to create tissue model function and the latter method to simultaneously fit multiple liver time–activity curves from images. The parameters obtained reproduced the DIF. Simulation studies were performed to examine the magnitude of potential biases in the flow values and to optimize the extraction of multiple tissue curves from the image.
*Results* The simulation showed that the error associated with assumed parameters was <10%, and the optimal number of tissue curves was between 10 and 20. The estimated DIFs were well reproduced against the measured ones. In addition, the calculated liver perfusion values were not different between the methods and showed a tight correlation ($r$=0.90).
*Conclusion* In conclusion, our results demonstrate that DIF can be estimated directly from tissue curves obtained through $H_2{}^{15}O$ PET imaging. This suggests the possibility to enable completely non-invasive technique to assess liver perfusion in patho-physiological studies.

**Keywords** Hepatic blood flow · Input function · Portal vein · Positron emission tomography · $H_2{}^{15}O$

N. Kudomi (✉) · L. Slimani · M. J. Järvisalo · R. Lautamäki · G. A. Naum · J. Knuuti · P. Nuutila · P. Iozzo
Turku PET Centre, University of Turku,
P.O. Box 52, 20521 Turku, Finland
e-mail: nobuyuki.kudomi@tyks.fi

J. Kiss · T. Savunen
Department on Surgery, University of Turku,
Turku, Finland

H. Iida
Department of Investigative Radiology,
Advanced Medical-Engineering Center,
National Cardiovascular Center-Research Institute,
5-7-1, Fujishirodai,
Suita, Osaka 565-8565, Japan

P. Nuutila
Department of Medicine, University of Turku,
Turku, Finland

P. Iozzo
Institute of Clinical Physiology, National Research Council,
56100 Pisa, Italy

## Introduction

The quantitative determination of hepatic blood flow has the potential to provide important information in the assessment and follow-up of liver disorders, which are almost invariably accompanied by abnormalities in organ

**Acknowledgement** This study was supported by the Budget for Nuclear Research of the Ministry of Education, Culture, Sports, and Technology (MEXT), Japan; a grant from the Cooperative Link of Unique Science and Technology for Economy Revitalization promoted by the Ministry of Education, Culture, Sports and Technology, Japan and a grant for translational research from the Ministry of Health, Labour and Welfare (MHLW), Japan. We would like to thank Nihon Medi-Physics, Hyogo, Japan for providing the $^{201}$Tl samples and also Mr. Yoshihide Takatani for his invaluable suggestion on the study design.

## References

1. Gullberg GT, Huesman RH, Ross SG, et al. Dynamic cardiac single-photon emission computed tomography. In: Beller GA, Zaret BL, editors. Nuclear cardiology: state of the art and future directions. Philadelphia, PA: Mosby-Year Book Inc.; 1998. p. 137–87.
2. Chiao PC, Ficaro EP, Dayanikli F, Rogers WL, Schwaiger M. Compartmental analysis of technetium-99m-teboroxime kinetics employing fast dynamic SPECT at rest and stress. J Nucl Med 1994;35(8):1265–73.
3. Narita Y, Eberl S, Iida H, Hutton BF, Braun M, Nakamura T, et al. Monte Carlo and experimental evaluation of accuracy and noise properties of two scatter correction methods for SPECT. Phys Med Biol 1996;41(11):2481–96.
4. Narita Y, Iida H, Eberl S, Nakamura T. Monte Carlo evaluation of accuracy and noise properties of two scatter correction methods for $^{201}$Tl cardiac SPECT. IEEE Trans Nucl Sci 1997;44:2465–72.
5. Iida H, Shoji Y, Sugawara S, Kinoshita T, Tamura Y, Narita Y, et al. Design and experimental validation of a quantitative myocardial $^{201}$Tl SPECT System. IEEE Trans Nucl Sci 1999;46:720–6.
6. Iida H, Narita Y, Kado H, Kashikura A, Sugawara S, Shoji Y, et al. Effects of scatter and attenuation correction on quantitative assessment of regional cerebral blood flow with SPECT. J Nucl Med 1998;39(1):181–9.
7. Kim KM, Watabe H, Hayashi T, Hayashida K, Katafuchi T, Enomoto N, et al. Quantitative mapping of basal and vasareactive cerebral blood flow using split-dose $^{123}$I-iodoamphetamine and single photon emission computed tomography. Neuroimage 2006;33(4):1126–35.
8. Beller GA, Watson DD, Pohost GM. Kinetics of thallium distribution and redistribution: clinical applications in sequential myocardial imaging. In: Pitt B, Strauss HW, editors. Cardiovascular nuclear medicine. St. Louis: Mosby; 1979. p 225–42.
9. Berman DS, Maddhi J, Garcia EV. Role of thallium-201 imaging in the diagnosis of myocardial ischemia and infarction. In: F HS, editor. Nuclear medicine annual. New York: Raven; 1980. p 1–55.
10. Weich HF, Strauss HW, Pitt B. The extraction of thallium-201 by the myocardium. Circulation 1977;56(2):188–91.
11. Camici PG, Crea F. Coronary microvascular dysfunction. N Engl J Med 2007;356(8):830–40.
12. Yokoyama I, Ohtake T, Momomura S, Nishikawa J, Sasaki Y, Omata M. Reduced coronary flow reserve in hypercholesterolemic patients without overt coronary stenosis. Circulation 1996;94 (12):3232–8.
13. Li J, Tsuji BMW, Welch A, Frey EC, Gullberg GT. Energy window optimization in simultaneous Technetium-99m and Thallium-201 SPECT data acquisition. IEEE Trans Nucl Sci 1995;42:1207–13.
14. Meikle SR, Hutton BF, Bailey DL. A transmission-dependent method for scatter correction in SPECT. J Nucl Med 1994;35(2):360–7.
15. Hudson HM, Larkin RS. Accelerated image reconstruction using srdered subsets of projection data. IEEE Trans Med Imag 1994;13:601–9.
16. Choi Y, Hawkins RA, Huang SC, Brunken RC, Hoh CK, Messa C, et al. Evaluation of the effect of glucose ingestion and kinetic model configurations of FDG in the normal liver. J Nucl Med 1994;35(5):818–23.
17. Hutton BF, Hudson HM, Beekman FJ. A clinical perspective of accelerated statistical reconstruction. Eur J Nucl Med 1997;24 (7):797–808.
18. Hutton BF, Lau YH. Application of distance-dependent resolution compensation and post-reconstruction filtering for myocardial SPECT. Phys Med Biol 1998;43(6):1679–93.
19. Pretorius PH, King MA, Pan TS, de Vries DJ, Glick SJ, Byrne CL. Reducing the influence of the partial volume effect on SPECT activity quantitation with 3D modelling of spatial resolution in iterative reconstruction. Phys Med Biol 1998;43(2): 407–20.
20. Soares EJ, Glick SJ, King MA. Noise chaeacterization of combined Bellini-type attenuation correction and frequency-distance principle restoration filtering SPECT. IEEE Trans Nucl Sci 1996;43:3278–90.
21. Iida H, Kanno I, Takahashi A, Miura S, Murakami M, Takahashi K, et al. Measurement of absolute myocardial blood flow with H215O and dynamic positron-emission tomography. Strategy for quantification in relation to the partial-volume effect. Circulation 1988;78(1):104–15.
22. Araujo LI, Lammertsma AA, Rhodes CG, McFalls EO, Iida H, Rechavia E, et al. Noninvasive quantification of regional myocardial blood flow in coronary artery disease with oxygen-15-labeled carbon dioxide inhalation and positron emission tomography. Circulation 1991;83(3):875–85.
23. Bergmann SR, Herrero P, Markham J, Weinheimer CJ, Walsh MN. Noninvasive quantitation of myocardial blood flow in human subjects with oxygen-15-labeled water and positron emission tomography. J Am Coll Cardiol 1989;14(3):639–52.
24. Iida H, Rhodes CG, de Silva R, Yamamoto Y, Araujo LI, Maseri A, et al. Myocardial tissue fraction-correction for partial volume effects and measure of tissue viability. J Nucl Med 1991;32(11): 2169–75.
25. Iida H, Tamura Y, Kitamura K, Bloomfield PM, Eberl S, Ono Y. Histochemical correlates of (15)O-water-perfusable tissue fraction in experimental canine studies of old myocardial infarction. J Nucl Med 2000;41(10):1737–45.
26. Iida H, Itoh H, Nakazawa M, Hatazawa J, Nishimura H, Onishi Y, et al. Quantitative mapping of regional cerebral blood flow using iodine-123-IMP and SPECT. J Nucl Med 1994;35(12):2019–30.
27. Onishi Y, Yonekura Y, Nishizawa S, Tanaka F, Okazawa H, Ishizu K, et al. Noninvasive quantification of iodine-123-iomazenil SPECT. J Nucl Med 1996;37(2):374–8.
28. Takikawa S, Dhawan V, Spetsieris P, Robeson W, Chaly T, Dahl R, et al. Noninvasive quantitative fluorodeoxyglucose PET studies with an estimated input function derived from a population-based arterial blood curve. Radiology 1993;188(1):131–6.
29. Fukushima K, Momose M, Kondo C, Kusakabe K, Kasanuki H. Myocardial kinetics of (201)Thallium, (99m)Tc-tetrofosmin, and (99m)Tc-sestamibi in an acute ischemia–reperfusion model using isolated rat heart. Ann Nucl Med 2007;21(5):267–73.
30. Lau CH, Eberl S, Feng D, Iida H, Lun PK, Siu WC, et al. Optimized acquisition time and image sampling for dynamic SPECT of Tl-201. IEEE Trans Med Imag 1998;17(3): 334–43.
31. Iida H, Itoh H, Bloomfield PM, Munaka M, Higano S, Murakami M, et al. A method to quantitate cerebral blood flow using a rotating gamma camera and iodine-123 iodoamphetamine with one blood sampling. Eur J Nucl Med 1994;21(10):1072–84.
32. Onishi Y, Yonekura Y, Mukai T, Nishizawa S, Tanaka F, Okazawa H, et al. Simple quantification of benzodiazepine receptor binding and ligand transport using iodine-123-iomazenil and two SPECT scans. J Nucl Med 1995;36(7):1201–10.

non-invasively from the SPECT data using, for example, a curve derived from a left ventricular region. However, it should be noted that the relationship between plasma and whole blood counts in this study was derived for a 4-min infusion protocol and may be different for other injection protocols, such as bolus injection. Previously, it has been shown that population-based input functions calibrated with one or two blood samples could avoid the need for frequent arterial blood samples [26–28]. There is also a potential for applying this approach to $^{201}$Tl studies. This is beyond the scope of this study and a systematic study should be designed to confirm this in clinical settings.

$^{201}$Tl has a high trans-capillary EF and thus the initial regional uptake of this tracer predominantly reflects the regional blood flow [10]. Use of a tracer that has a high first-pass EF is essential when one intends to quantitatively assess MBF at a high flow range or the coronary flow reserve. The EF of $^{201}$Tl is reported as >0.8 [10] for a wide flow range and is known to be higher than $^{99m}$Tc-labelled tracers such as tetrofosmine and sestamibi [29]. The physical characteristics of $^{201}$Tl are unfortunately not ideal as low energy emission increases the attenuation factor and the scatter in the image. In addition, the relatively long half-life limits the administered activity to about a tenth of that with $^{99m}$Tc tracers. Despite these shortcomings, the physiological characteristics of having high first-pass EF make $^{201}$Tl an interesting tracer particularly for the absolute quantitation of MBF and the coronary flow reserve. This study demonstrates that quantitative physiological parameters can be derived from dynamic $^{201}$Tl SPECT studies, despite its less than ideal imaging characteristics.

Whilst the quantitative physiological parameter estimation removed the systematic bias between MBF estimated by $^{201}$Tl dynamic SPECT and by microspheres, the spread of data points around the regression line was rather large (Figs. 6e and 7c). This is not only due to possible errors in the estimation of MBF from the $^{201}$Tl, but there was also considerable variation in flow estimated by the microspheres at the beginning and end of the study. Thus, at least part of the variability is attributable to errors in microsphere flow measurement, and particularly for the pharmaceutical intervention studies, flow may not have remained constant throughout the entire study duration, which may also account for some of the differences seen between the various flow measurements.

$V_d$ estimated in this study could serve as an index of viability, as viable myocytes are required to maintain the large concentration gradient between plasma and myocardium at equilibrium. There was no significant difference in $V_d$ values between rest, beta-blocker and adenosine studies when fitted for 1 h (Fig. 8). The significant difference between the 1- and 4-h fit for resting data could be explained by the limitation of the two-compartment model. Considerable spread in the $V_d$ values observed over all dog studies on the other hand was partially attributed to the short (insufficient) scan time for reliable estimates of $V_d$. With the exception of the large, outlying $V_d$ values in all 5 regions of 1 dog, the resting $V_d$ values fell within a relatively narrow range of 47 to 65 (mean±SD=55±6). Given the sufficiently long scan time, significant reduction in $V_d$ in infarcted areas may be detected. However, this would need to be tested with a suitable study design.

The scan time of 4 h required to achieve reliable $V_d$ estimates is not practical in the routine clinical setting. As has been shown by Lau et al. [30], the scan period may be split into two sessions, an early dynamic scan for 30 min followed by a single static scan at approximately 3 h. This scheme is not more onerous than current rest/re-distribution protocols and hence could be practical. In addition, it may be possible to simplify the scanning protocol further to two static scans by using the table look-up method for the two-compartment model, which has been successfully employed for other SPECT tracers with relatively slow kinetics similar to $^{201}$Tl [27, 31, 32]. This warrants further investigation.

This study relies on established, rigorous attenuation and scatter correction in SPECT [5] and availability of multi-detector SPECT systems capable of performing dynamic acquisition. To our knowledge, this is the first report that has demonstrated that it is possible to obtain quantitative physiological parameter estimates of $K_1$ and $V_d$ in the myocardium using a clinical SPECT scanner and $^{201}$Tl. This work suggests that it is feasible to apply our technique to clinical studies. Further studies are, however, needed to validate the proposed approach in the clinical setting. Incomplete motion correction is one possible error source, particularly in patients. Dynamic SPECT is probably more sensitive to the possible movement of patients during the study. Shortened clinical protocol is preferred, but this requires additional development to improve the reliability of parameter estimates. In addition, two scanning sessions are needed to assess the coronary flow reserve. We have recently demonstrated a technique to assess two cerebral blood flow images, one at rest and another after a vasodilating drug, from a single session of a SPECT scan in conjunction with split dose administration of $^{123}$I-iodoamphetamine and dynamic SPECT [7]. As a clinical implication, the quantitative assessment of MBF and coronary flow reserve is important. For instance, coronary micro-vascular dysfunction or impaired endothelial function in patients with coronary risk factors or patients with cardiomyopathy or with heart failure is an un-resolved important issue to answer [11]. Coronary flow reserve can be reduced in patients with hypercholesterolemia without overt coronary stenosis [12]. A systematic study should be carried out to validate this approach for assessing MBF at rest and after adenosine from a single session of a scan.

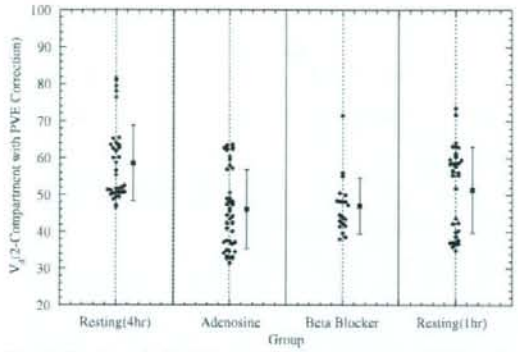


**Fig. 8** $V_d$ values obtained from the two-compartment model fit to the full 4 h resting data, adenosine and beta-blocker infusion 1 h curves and fit to first 1 h only of the resting study curves. Data from the multiple individual myocardial regions are shown

Figure 8 plots the $V_d$ values for all evaluated myocardial segments for the fit to 4 h resting data, adenosine and beta-blocker infusion 1 h data and fit to only the first 1 h of resting data. The 4-h resting $V_d$ values are significantly higher ($p<0.01$) compared with the adenosine, beta-blocker values and compared with the fit to the first 1 h resting data. However, the 1-h resting values are not significantly different from the beta-blocker $V_d$ values nor the adenosine values.

## Discussion

This study demonstrates that the kinetic analysis of quantitatively assessed myocardial $^{201}$Tl accumulation (build-up and washout in healthy canines) provided quantitative MBF values, which agreed well with flows obtained using microspheres for a wide physiological range of flows. The size of the TTACs relative to the arterial plasma concentration corresponded well to the pharmacological stresses induced by adenosine and beta-blocker challenges. The compartmental model approach could reproduce these TTACs to make the determination of kinetic parameters, such as $K_1$ and $V_d$, possible. The three-compartment model gave results which were generally higher than the two-compartment model and which were statistically significantly better in terms of AIC, SC for the resting and adenosine studies, and this was in line with the visual inspection of the TTAC model fit curves. It should, however, be noted that the differences were only small between the two- and three-compartment model approaches, approximately 20% for $K_1$ and 10% for $V_d$ The bias associated with the two-compartment model could be corrected by a linear regression as shown in Fig. 7a–c. This opens the possibility of using the more reliable two-compartment model fit due to its reduced number of parameters for routine clinical studies. The improved reliability of the two-compartment model fit in the clinical setting is particularly important if one intends to shorten the study time or generate parametric images.

The three corrections for PVE, Hct and first-pass EF proved to be important. The PVE correction method used in this work cannot, however, be applied to clinical studies, and the PVE correction in the beating heart still remains a considerable challenge in clinical studies. PVE may be reduced by gating the data, which may not, however, be feasible for the already noisy and large dynamic SPECT data sets. PVE may also be reduced by including resolution recovery as part of the reconstruction process [17–20]. Alternatively, it may also be possible to include PVE as part of the kinetic model fitting [21–25]. However, this adds extra fitting parameters and requires some parameters to be assumed fixed.

The input function is an important component in compartment model fitting. In this study, rapid arterial blood sampling was performed, and the plasma was separated by centrifugation. A number of important insights were gained by performing rapid separation of plasma in a subset of samples and dogs. It was found that $^{201}$Tl enters the red blood cells as observed from the rapid separation of plasma in a subset of samples and dogs, which is not un-expected as potassium is also known [22] to be taken up by the red blood cells. The exchange of $^{201}$Tl between red blood cells and plasma is relatively slow compared to the passage of blood through the capillary bed and hence direct uptake of activity from the red blood cells into tissue is believed to be negligible. Hence, tissue uptake will be dominated by the activity in the plasma during passage through the capillary bed and plasma in the substrate being measured. As a consequence, the flow measurement obtained with $^{201}$Tl is plasma flow, which is in contrast to the microsphere studies, which measure whole blood flow. Conversion of plasma to blood flow was achieved by dividing the plasma flow by (1−Hct), as shown in Eq. 1, which then allowed the direct comparison with the microsphere measurements.

Rigorous estimation of the input function requires frequent arterial blood sampling. This is not only considered invasive, but also labor intensive. In addition, it has been shown in this study that rapid separation of the plasma for at least the first 30–40 min post-$^{201}$Tl administration is required to obtain accurate plasma concentration. If the separation of plasma is delayed, then the true plasma concentration at the time of sampling cannot be measured, which results in biased $K_1$ estimates. An empirical relationship of plasma to whole blood ratio as a function of time was developed and was found to be sufficiently consistent between dogs (Fig. 3) to allow the mean curve to be applied with minimal bias. Thus, in clinical practice, whole blood samples may be counted and converted to plasma concentration using the empirical relationship. This also potentially allows the input function to be obtained